PCCP

PAPER

View Article Online
View Journal | View Issue

Cite this: *Phys. Chem. Chem. Phys.*, 2015, **17**, 896

Electronic structures at the interface between Au and $CH_3NH_3PbI_3$

Xiaoliang Liu,[a] Chenggong Wang,[b] Lu Lyu,[a] Congcong Wang,[b] Zhengguo Xiao,[c] Cheng Bi,[c] Jinsong Huang[c] and Yongli Gao*[b]

Received 27th August 2014, Accepted 4th November 2014

DOI: 10.1039/c4cp03842h

www.rsc.org/pccp

The electronic properties of interfaces formed between Au and organometal triiodide perovskite ($CH_3NH_3PbI_3$) are investigated using ultraviolet photoemission spectroscopy (UPS), inverse photoemission spectroscopy (IPES) and X-ray photoemission spectroscopy (XPS). It is found that the $CH_3NH_3PbI_3$ film coated onto the substrate of poly(3,4-ethylenedioxythiophene) poly(styrenesulfonate) (PEDOT:PSS)/indium tin oxide (ITO) by a two-step method presents n-type semiconductor behavior, with a band gap of 1.7 eV and a valence band (VB) edge of 1.0 eV below the Fermi energy (E_F). An interface dipole of 0.1 eV is observed at the $CH_3NH_3PbI_3$/Au interface. The energy levels of $CH_3NH_3PbI_3$ shift upward by *ca.* 0.4 eV with an Au coverage of 64 Å upon it, resulting in band bending, hence a built-in field in $CH_3NH_3PbI_3$ that encourages hole transport to the interface. Hole accumulation occurs in the vicinity of the interface, facilitating the hole transfer from $CH_3NH_3PbI_3$ to Au. Furthermore, the shift of the VB maximum of $CH_3NH_3PbI_3$ toward the E_F indicates a decrease of energy loss as holes transfer from $CH_3NH_3PbI_3$ to Au.

1. Introduction

Recently, there has been an unexpected breakthrough and rapid evolution of highly efficient solid-state hybrid solar cells based on organometal trihalide perovskite materials.[1–8] The breakthrough has the potential to produce solar cells with very high efficiencies while retaining a very low cost. Kojima *et al.*[9] first reported in 2009 on a 3.5% efficient sensitized solar cell with a TiO_2, $CH_3NH_3PbI_3$, and iodide/triiodide redox couple. Im *et al.*[10] improved the sensitized solar cell by optimizing the TiO_2 surface and perovskite processing, reporting a 6.5% $CH_3NH_3PbI_3$ liquid electrolyte solar cell. Kim *et al.*[11] and Lee *et al.*[12] developed solid-state perovskite solar cells employing 2,2′,7,7′-tetrakis-(*N,N*-di-*p*-methoxyphenyl-amine)-9,9′-spirobifluorene (spiro-OMeTAD) as the hole transporter, and presented efficiencies between 8% and 10% with $CH_3NH_3PbI_3$ and $CH_3NH_3PbI_{3-x}Cl_x$ mixed halide perovskite, respectively. By depositing PbI_2 on nanoporous TiO_2 and subsequently submerging it into a CH_3NH_3I solution, Grätzel and his co-workers[13] brought the efficiency to 15%. Using vapor deposition, Snaith's group demonstrated that a planar heterojunction perovskite solar cell, without the mesoporous electrode in typical sensitized solar cells, could have a very high efficiency of 15%.[14,15] It is expected that the efficiency of 20% or higher can be reached by optimizing the device structures. In addition, it was also shown that one of the most striking aspects of the perovskites is that the cells could generate a very high open-circuit voltage (V_{oc}), and that the materials exhibited sufficiently good ambipolar charge transport for electrons and holes.[11,16] Given the high efficiency and inexpensive materials and processing, it is forecasted that a new wave of research and development of perovskite solar cells will bring many transformative steps over the coming years and a tangible possibility in making solar energy as the lowest-cost energy source.

In spite of many achievements in the application of organometal halide perovskite-based organic planar heterojunction solar cells, the basic energetics of these systems still remains unsolved, such as the positions of the electronic band edges and their alignment with the energy levels of adjacent layers. To understand the mechanism and to optimize the device structure of organometal trihalide perovskite-based organic solar cells, it is imperative to learn the precise role of each interface in the device architecture.

In solar cells based on organometal halide perovskite, Au is most widely used as an electrode. It is believed that a typical planar structure of Au/$CH_3NH_3PbI_3$ and an electron transport layer such as C_{60} can be used to build an effective solar cell. To understand the electronic structure and the carrier transfer mechanism at the $CH_3NH_3PbI_3$/Au interface, we report our study using ultraviolet photoemission spectroscopy (UPS), inverse photoemission spectroscopy (IPES) and X-ray photoemission

[a] *Hunan Key Laboratory for Super-microstructure and Ultrafast Process, College of Physics and Electronics, Central South University, Changsha, 410083, P. R. China*
[b] *Department of Physics and Astronomy, University of Rochester, Rochester, NY 14627, USA. E-mail: ygao@pas.rochester.edu*
[c] *Department of Mechanical and Materials Engineering and Nebraska Center for Materials and Nanoscience, University of Nebraska-Lincoln, Lincoln, Nebraska 68588-0656, USA*

spectroscopy (XPS) on this interface. We measured directly the evolution of energy levels as Au was deposited successively layer by layer on a $CH_3NH_3PbI_3$ film. The Au electrode lifted efficiently the energy levels of $CH_3NH_3PbI_3$ and a small energy offset of 0.6 eV was observed between the valence band (VB) edge of $CH_3NH_3PbI_3$ and the Fermi energy (E_F) of the system, indicating a weak energy loss as holes transfer from $CH_3NH_3PbI_3$ to Au. Au clusters formed on the top of the $CH_3NH_3PbI_3$ film were observed at lower Au coverages, leading to an initial charging of 0.3 eV. These investigations provide some insight into the understanding of Au/$CH_3NH_3PbI_3$-based organic solar cells.

2. Results and discussion

Shown in Fig. 1 is the XPS full scan spectrum of the $CH_3NH_3PbI_3$ film on top of an ITO/PEDOT:PSS substrate. As expected, the sample displays carbon, nitrogen, iodine and lead, and the surface composition C : N : Pb : I = 0.9 : 0.8 : 1 : 2.4 can be confirmed by the core level intensity, indicating a bit of deviation from the stoichiometry of $CH_3NH_3PbI_3$. We obtained the areas of the XPS spectra of these elements by fitting Gaussian peaks after removing the secondary electron background, followed by normalization with corresponding atomic sensitivity factors. The relatively low proportions of nitrogen, carbon and iodide can be perhaps attributed to the deficiency of CH_3NH_3I. The $CH_3NH_3PbI_3$ is not thermally stable at temperatures above 150 °C due to its low dissociation energy.[20–22] Thermal annealing is a necessary step in the fabrication process of perovskite films in order to have enough interdiffusion between CH_3NH_3I and PbI_2. However, thermal annealing may also dissociate $CH_3NH_3PbI_3$ partly into PbI_2 and CH_3NH_3I, and the CH_3NH_3I may subsequently evaporate, resulting in reduced N content.

In Fig. 2, the evolution of the UPS spectra is presented as a function of the thickness of Au deposited on the $CH_3NH_3PbI_3$ film. For visual clarity, we normalized all the spectra to the same height. Shown in Fig. 2(a) are the UPS data of the cut-off region with the binding energy (BE) from the E_F of the system. The cut-off energy is determined by the inflection point of the sharp change region of the cut-off spectrum.[23–25] Then the vacuum level (VL) is obtained from the difference between the photon energy (21.22 eV) and the cut-off energy. The VL of $CH_3NH_3PbI_3$ film is measured to be 4.7 eV above the E_F, *i.e.*, the work function (WF), and it decreases to 4.4 eV upon the deposition of 0.5 Å Au. With the subsequent deposition of Au, the VL increases rapidly at first, and then more gradually. It finally saturates at 5.2 eV with an Au coverage of 64 Å. Fig. 2(b) presents the UPS data of the highest lying VB regions, in which the VB maximum (VBM) of $CH_3NH_3PbI_3$ film displays *ca.* 1.0 eV. The VB edges are obtained using linear extrapolation as illustrated in our previous studies.[26,27] As more Au is deposited, a finite density of valence states is observed within the gap of $CH_3NH_3PbI_3$. The density of valence states is faint at first, and then it extends up to E_F as the Au coverage reaches *ca.* 8 Å and a true metallic Fermi edge develops completely with the Au deposition of up to Θ = 64 Å. This effect is just similar to that confirmed by Dürr *et al.*[28] as Au was deposited on diindenoperylene (DIP).

Notably, a sharp shift of *ca.* 0.3 eV toward high BE is observed from the UPS spectra of the cut-off region and the VB edge region at 0.5 Å Au deposition upon $CH_3NH_3PbI_3$ film, which can be ascribed to sample charging during UPS at lower Au coverage. As reported by Koch *et al.*[29] and Oji *et al.*[30] Au clusters formed on some organic films as Au was deposited upon them with a lower Au overlayer. Here, small Au clusters formed on the top of the $CH_3NH_3PbI_3$ film make it difficult to transfer electrons from $CH_3NH_3PbI_3$ to the Au clusters to establish charge neutrality, resulting in a positive charge of *ca.* 0.3 eV on the Au clusters, hence the same amount of energy level shift toward higher BE. However, upon the subsequent Au deposition, the UPS spectra shift back to lower BE, indicating that thicker Au films eliminate the charging. This process can be interpreted by percolation theory. Most clusters on the top of $CH_3NH_3PbI_3$ film are too small to be metallic at first, and then an increasing number of the clusters become large enough to percolate, thus to exhibit metallic character. Shown in Fig. 2(c) is the local enlarged view of the VB edge region near E_F. We observe here that the Fermi edge actually is visible even for 2 Å of Au. At this phase the Fermi edge locates 0.2 eV below the E_F of the system due to charging. During the process of the subsequent Au deposition, it shifts back toward the E_F because of the elimination of the charging induced by the Au cluster percolation (see the dotted lines in Fig. 2(c)). Upon the deposition of *ca.* 8 Å Au, the shift of the Fermi edge almost saturates and a continuous metal surface coverage and conductivity are achieved.

To obtain the detailed information on the unoccupied states of $CH_3NH_3PbI_3$, we further collected the IPES data of the pristine $CH_3NH_3PbI_3$ film. The IPES spectrum is presented in Fig. 2(d). The conduction band minimum (CBM) is measured to be 0.7 eV above the Fermi level (E_F), while the VBM is 1.0 eV below the E_F, corresponding to a gap of 1.7 eV, which is consistent with previous reports.[31] Interestingly, the $CH_3NH_3PbI_3$ film measured here presents an n-type semiconductor behavior. It is possible

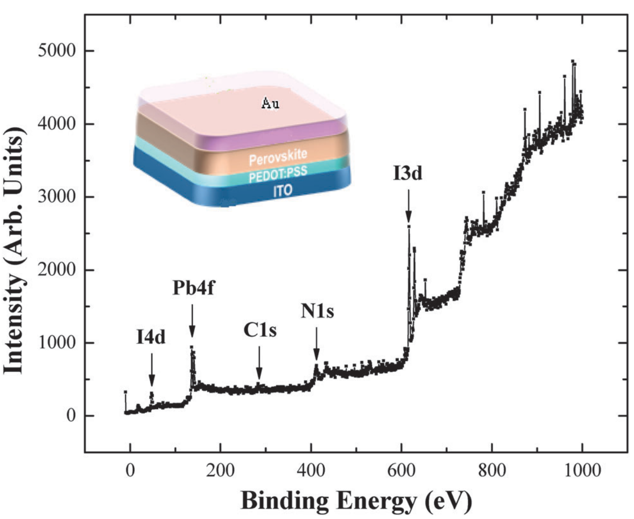

Fig. 1 X-ray photoemission spectroscopy of the $CH_3NH_3PbI_3$ film on the top of the ITO/PEDOT:PSS substrate. Inset: the schematic diagram of the structure of ITO/PEDOT:PSS/$CH_3NH_3PbI_3$/Au.

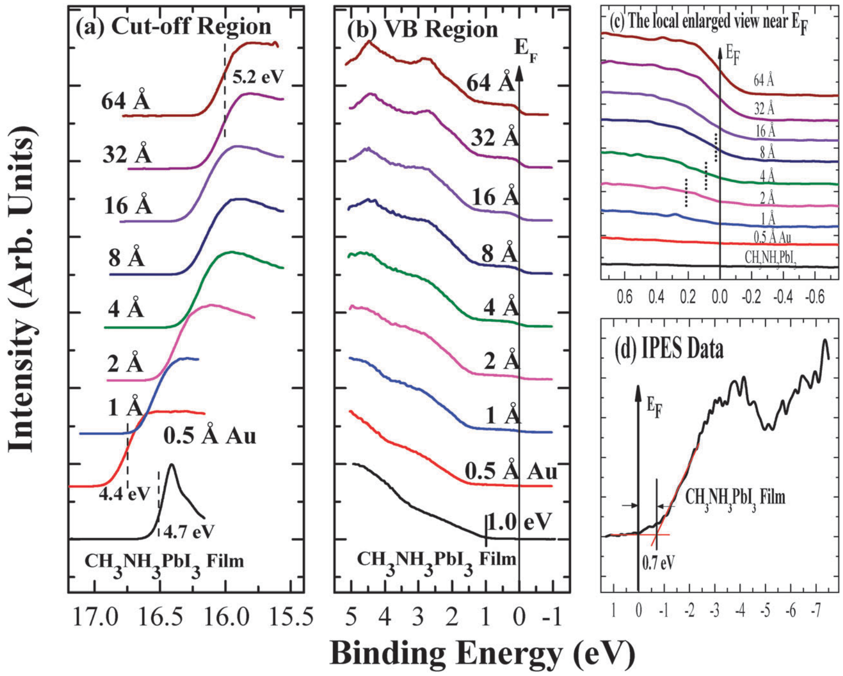

Fig. 2 Thickness dependent UPS spectra of Au on $CH_3NH_3PbI_3$ coated on the PEDOT:PSS/ITO substrate showing (a) the cut-off region, (b) the VB edge region, and (c) the local enlarged view of the VB edge region near E_F. (d) presents IPES spectra of the density of states close to the bandgap of $CH_3NH_3PbI_3$. Positions of the VB edge and the CB edge are marked with vertical bars, while positions of the cut-off energy and the Fermi edge are marked with dashed and dotted lines, respectively.

that the conductivity type, *i.e.*, n-type or p-type, can be tuned by the film formation composition and thermal annealing process.

The positive charging induced by Au clusters at lower Au coverage is also confirmed by the XPS spectra. Shown in Fig. 3 are the evolutions of C 1s, I 3d, Pb 4f and Au 4f XPS peaks as a function of increasing Au coverage. All the spectra were normalized to the same height. The BE of the peak center was obtained by Gaussian fitting. The dashed lines mark the core levels C 1s, I 3d and Pb 4f of the pristine $CH_3NH_3PbI_3$ film. In Fig. 3(a)–(c), the core levels of C 1s, I 3d and Pb 4f shift simultaneously 0.3 ± 0.1 eV toward higher BE resulting from the initial charging at $\Theta = 0.5$ Å. Then, following the same manner of the VL and the VBM of $CH_3NH_3PbI_3$ presented by UPS spectra, they shift toward lower BE with more Au deposition as the charging is being eliminated. It is observed that an Au coverage of about 8 Å can eliminate the charging and shift the core levels of C 1s, I 3d and Pb 4f back to the original position of the pristine $CH_3NH_3PbI_3$ film. In addition, as shown in Fig. 3(d), the evolution of the Au 4f peak provides further evidence for positive charging. We obtained the highest BE of Au 4f at the initial $\Theta = 0.5$ Å of Au coverage due to the positive charging, then this core level shifts downward gradually as the charging is gradually eliminated by further Au deposition. Moreover, we also observed the broadening of the XPS spectra at $\Theta = 0.5$–2 Å of Au deposition, which is another evidence supporting the existence of Au clusters.[28] Notably, the core levels of C 1s, I 3d and Pb 4f shift back to lower BE by *ca.* 0.4 eV with an Au coverage of 64 Å relative to the pristine $CH_3NH_3PbI_3$ film.

In Fig. 4, we present directly the relative shifts of the VL and core levels at the $CH_3NH_3PbI_3$/Au interface as a function of Au coverage. The core levels of C 1s, I 3d and Pb 4f shift almost the same as the VL, indicating no significant surface chemical modification during this deposition process. As discussed in the previous section, the energy levels shift toward higher BE upon small Au depositions, and shift back to the original position with an Au coverage of *ca.* 8 Å due to the elimination of charging. They then shift sequentially toward lower BE with enough thickness of Au deposition.

Generally, to obtain the true information on the energy level positions, the charging effect must be removed. Koch *et al.*[32] introduced a technique to eliminate the charging by irradiating the sample with light of appropriate wavelength. But in this paper, it is unnecessary to eliminate the charging by using an extra technique since the charging is naturally eliminated with the Au deposition of up to 8 Å and the impact of charging on the energy level can be ignored with enough Au coverage. The rigid shifts of core levels saturated at *ca.* 0.4 eV lower BE with respect to the initial core levels in $CH_3NH_3PbI_3$ film, indicating the upward shift of energy levels, thus, the band bending in $CH_3NH_3PbI_3$ film induced by the Au coverage.

The energy level alignment diagram at $CH_3NH_3PbI_3$/Au interfaces is depicted in Fig. 5. The VL and CBM of pristine $CH_3NH_3PbI_3$ film obtained from Fig. 2(a) and (d) are 4.7 and 0.7 eV above the E_F, respectively, while the VBM obtained from Fig. 2(b) is 1.0 eV below the E_F. A gradual energy level shift is observed with the subsequent Au depositions. We neglected the intermediate charging processes because it was naturally eliminated without a significant impact on the final energy levels. On the side of $CH_3NH_3PbI_3$, at the very interface of $CH_3NH_3PbI_3$/Au, the VL,

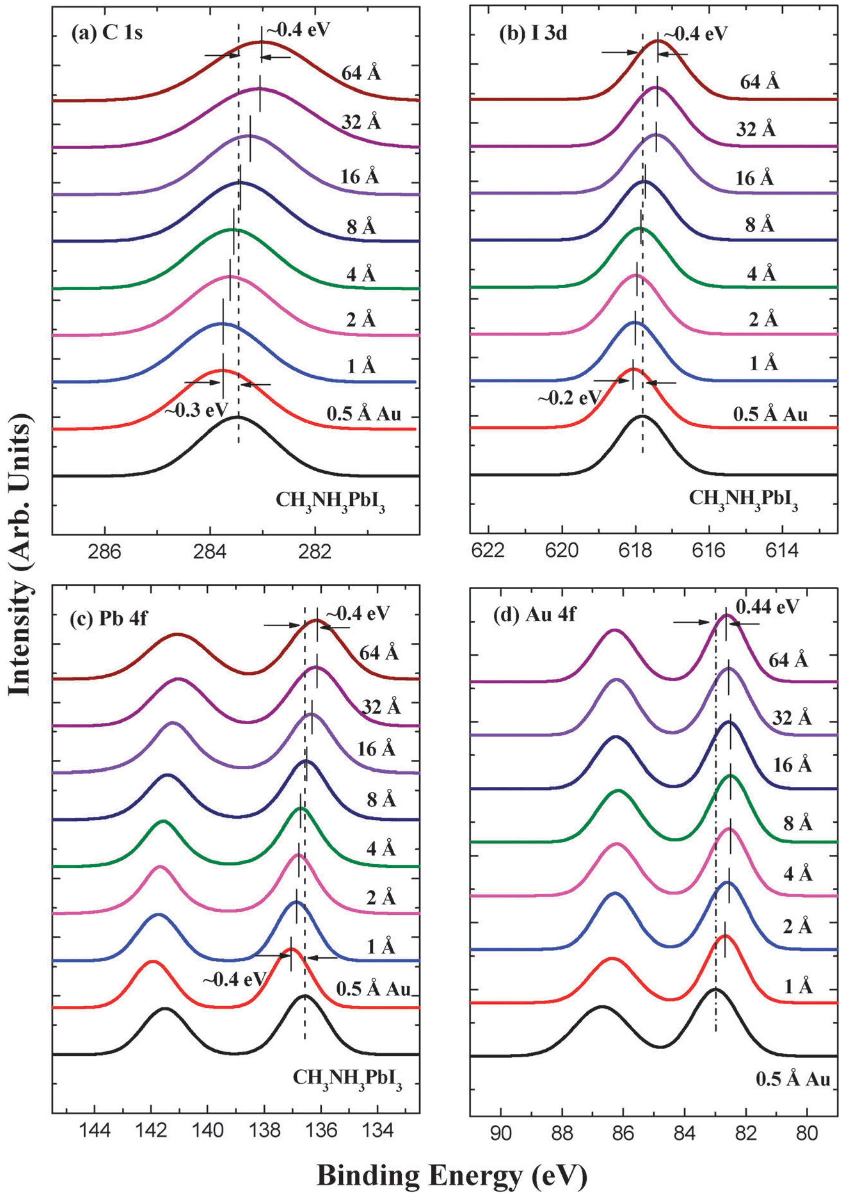

Fig. 3 The evolution of (a) C 1s, (b) I 3d and (c) Pb 4f XPS peaks in the $CH_3NH_3PbI_3$ film, and that of (d) Au 4f XPS peaks in Au coverage, with the increasing Au coverage thickness.

CBM and VBM of $CH_3NH_3PbI_3$ are 5.1, 1.1 eV above, and 0.6 eV below the E_F, respectively, after considering the 0.4 eV upward shift of energy levels with respect to the final deposition of 64 Å Au. On the side of Au, the VL is 5.2 eV according to the UPS data in Fig. 2, which indicates that there is an interface dipole of 0.1 eV at the interface of $CH_3NH_3PbI_3$/Au ascribed to the difference of WF between $CH_3NH_3PbI_3$ and Au. The VBM of $CH_3NH_3PbI_3$ is brought to the E_F of the system, resulting in band bending as mentioned in the previous subsection, and thus a built-in field in the $CH_3NH_3PbI_3$ film that encourages hole transport to the interface. The hole accumulation in the vicinity of the interface facilitates the hole transfer from $CH_3NH_3PbI_3$ to Au. Furthermore, the decreasing energy offset between the VBM of $CH_3NH_3PbI_3$ and the E_F indicates a decreasing energy loss for hole extraction from $CH_3NH_3PbI_3$ to the Au. Given the favorable energy level alignment, the $CH_3NH_3PbI_3$/Au interface can be effectively used as hole collectors in perovskite-based solar cells.

In order to further ascertain the process of the growth of Au on $CH_3NH_3PbI_3$ film, we focus on the XPS intensity attenuation by the Au overlayer. For the elements in the $CH_3NH_3PbI_3$ substrate, the intensity attenuation of photoelectrons after passing through an Au overlayer of thickness d is given by[33]

$$I_s = I_{s0}\exp(-d/\lambda_s), \qquad (1)$$

where I_{s0} and I_s are the original and attenuated photoelectron intensities, respectively, and λ_s is the mean free path (MFP) of photoexcited electrons in Au.

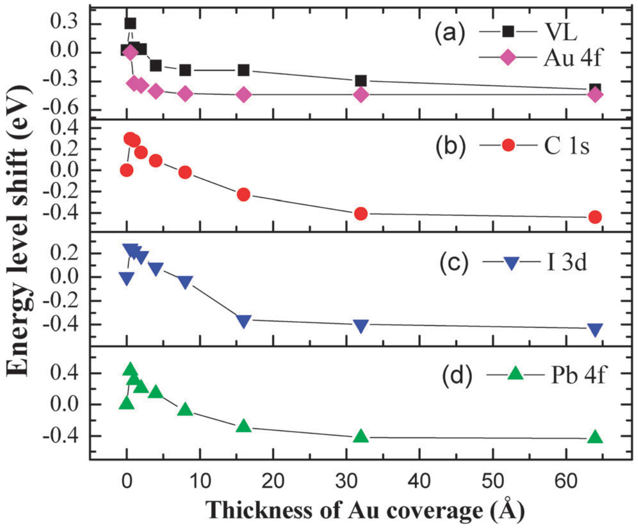

Fig. 4 The relative shifts of the vacuum level and core levels at the $CH_3NH_3PbI_3$/Au interface deduced from UPS and XPS. The zero of the energy scale refers to the value of zero (or 0.5 Å for Au 4f) Au coverage.

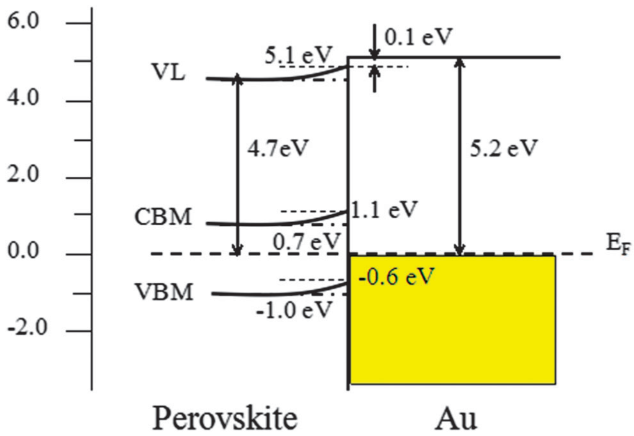

Fig. 5 The energy level diagram of the $CH_3NH_3PbI_3$/Au interface. The dashed dotted lines denote the energy levels of the pristine $CH_3NH_3PbI_3$ film, while the solid lines on the side of $CH_3NH_3PbI_3$ denote the evolution of the energy levels with the deposition of Au.

The photoelectron intensity is obtained based on the peak area and after proper normalization using atomic sensitivity factors. As shown in Fig. 6, for the photoelectrons ejected from the C 1s, I 3d and Pb 4f of the $CH_3NH_3PbI_3$ film, the intensities attenuate gradually with increasing thickness of Au coverage up to 8 Å, and decrease sharply with thicker Au coverage, which can be also attributed to the effect of Au clusters. The slight differences in the shape among the three curves arise from the slightly different kinetic energies of the electrons ejected from the three core levels. The formation of Au clusters at lower Au coverages, *i.e.* $\Theta < 8$ Å, exposes a larger surface area of the underlying $CH_3NH_3PbI_3$ film than an evenly distributed Au film, thereby the photoelectron intensity decreases gently at first, which can be confirmed by a small slope for the C 1s as shown with a dash line in the figure. The slope curve is obtained by linearly fitting the experimental data of $\Theta < 8$ Å.

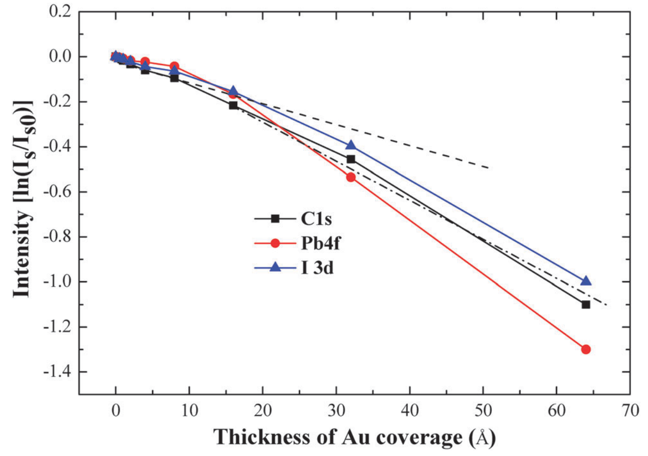

Fig. 6 The photoelectron intensity as a function of the thickness of Au coverage. The dashed line and the dashed dotted line mark the slopes for the C 1s before and after the Au deposition of 8 Å, respectively.

However, with enough thickness of the Au coverage, *i.e.* $\Theta > 8$ Å, the Au clusters percolate and a continuous metal Au surface coverage is formed on the top of the $CH_3NH_3PbI_3$ film. Thus, the photoelectrons ejected from the underlying $CH_3NH_3PbI_3$ film are significantly suppressed by the Au coverage and a sharper decrease of photoelectron intensity is certainly achieved by subsequent deposition of Au, which can also be confirmed by a relatively big slope for the C 1s as shown with a dashed dotted line in the figure.

3. Experimental method

Preparation of $CH_3NH_3PbI_3$ film

$CH_3NH_3PbI_3$ film was prepared by using a two step technique as recently reported.[13,17–19] Shortly, poly(3,4-ethylenedioxythiophene) poly(styrenesulfonate) (PEDOT:PSS) was spun coated onto the ITO substrate at 3000 rpm for 60 s, and then followed by 135 °C annealing for 20 min. PbI_2 precursor solution obtained by dissolving PbI_2 in anhydrous DMF was spun onto the ITO/PEDOT:PSS substrate at 70 °C with 6000 rpm for 45 s, and the as-prepared PbI_2 film was then dried at 70 °C for 15 min. The CH_3NH_3I layer was prepared by spin coating the CH_3NH_3I precursor solution obtained by dissolving CH_3NH_3I in 2-propanol onto the top of PbI_2 film at a rate of 6000 rpm for 35 s at room temperature. After the deposition of the CH_3NH_3I layer, the PbI_2/CH_3NH_3I stacking film was dried in a hot plate at 75 °C for 15 min, and then annealed at 105 °C for 2 hours.

Material characterization

Au was degassed at proper temperatures before evaporation. 0–64 Å Au films were thermally evaporated layer by layer in the metal evaporation chamber onto ITO/PEDOT:PSS/$CH_3NH_3PbI_3$ (see inset in Fig. 1). The thickness of evaporated film was monitored with a quartz crystal microbalance. The deposition rate of Au was 0.2 Å s^{-1}. The UPS and XPS spectra were recorded at each step, while IPES spectra were just collected for as-grown $CH_3NH_3PbI_3$ film. The XPS and UPS experiments were performed using a VG ESCA Lab system equipped with a He I (21.2 eV) gas discharge lamp and a Mg K_α X-ray source (1253.6 eV). The IPES spectra were recorded using a custom-made spectrometer, composed of a commercial Kimball Physics ELG-2 electron gun and a band pass photon detector. The photon detector worked in the isochromatic mode centered at a fixed energy of 9.8 eV. The instrumental resolution for UPS measurements was chosen to be 0.20 eV and the XPS resolution is *ca.* 1.4 eV. The combined resolution (electron + photon) of the IPES spectrometer was determined to be *ca.* 0.6 eV. All measurements were done at room temperature.

4. Conclusions

In conclusion, we have investigated the electronic properties of the $CH_3NH_3PbI_3$/Au interface using UPS, XPS and IPES. Au can efficiently lift the energy level of $CH_3NH_3PbI_3$ film by 0.4 eV, resulting in band bending and thus a built-in field in $CH_3NH_3PbI_3$. The enhanced hole accumulation at the very interface due to the p-type self-doping behavior facilitates the hole transfer from $CH_3NH_3PbI_3$ to Au. The energy loss decreases significantly as hole extraction takes place from $CH_3NH_3PbI_3$ to the Au electrode due to the decreasing offset between the VBM of $CH_3NH_3PbI_3$ and the E_F of the system. Even though for an n-typed $CH_3NH_3PbI_3$, it is confirmed that the $CH_3NH_3PbI_3$/Au interface can be effectively used as hole collectors in a perovskite-based solar cell, indicating the huge potential of $CH_3NH_3PbI_3$/Au-based organometal trihalide perovskite planar structured solar cells. Furthermore, an initial charging of 0.3 eV observed with the deposition of lower Au coverage can be attributed to Au clusters formed on the top of the $CH_3NH_3PbI_3$ film. The charging will be eliminated with a thicker Au coverage of *ca.* 8 Å following a metallic Fermi edge emergence. These investigations provide some insight into the understanding of $CH_3NH_3PbI_3$/Au-based organic planar heterojunction solar cells.

Acknowledgements

This work is supported in part by the National Science Foundation (Grant No. CBET-1437656) and the National Natural Science Foundation of China (Grant No. 51173205, 11334014). One of us (X. L. Liu) acknowledges support from the Natural Science Foundation of Hunan Province, China (Grant No. 12JJ3003) and the Freedom Explore Program of Central South University, China (Grant No. 2011QNZT122).

Notes and references

1 E. Edri, S. Kirmayer, D. Cahen and G. Hodes, *J. Phys. Chem. Lett.*, 2013, **4**, 897–902.
2 P. Docampo, J. M. Ball, M. Darwich, G. E. Eperon and H. J. Snaith, *Nat. Commun.*, 2013, **4**, 2761.
3 J.-H. Qiu, Y.-C. Qiu, K.-Y. Yan, M. Zhong, C. Mu, H. Yan and S.-H. Yan, *Nanoscale*, 2013, **5**, 3245–3248.
4 L. Etgar, P. Gao, Z.-S. Xue, Q. Peng, A. K. Chandiran, B. Liu, M. K. Nazeeruddin and M. Grätzel, *J. Am. Chem. Soc.*, 2012, **134**, 17396–17399.
5 D. B. Mitzi, S. Wang, C. A. Feild, C. A. Chess and A. M. Guloy, *Science*, 1995, **267**, 1473–1476.
6 J.-Y. Jeng, Y.-F. Chiang, M.-H. Lee, S.-R. Peng, T.-F. Guo, P. Chen and T.-C. Wen, *Adv. Mater.*, 2013, **25**, 3727–3732.
7 G. C. Xing, N. Mathews, S. Y. Sun, S.-S. Lim, Y.-M. Lam, M. Grätzel, S. Mhaisalkar and T.-C. Sum, *Science*, 2013, **342**, 344–347.
8 J. A. Mikroyannidis, A. N. Kabanakis, S. S. Sharma and G. D. Sharma, *Adv. Funct. Mater.*, 2011, **21**, 746–755.
9 A. Kojima, K. Teshima, Y. Shirai and T. Miyasaka, *J. Am. Chem. Soc.*, 2009, **131**, 6050.
10 J. H. Im, C. R. Lee, J. W. Lee, S. W. Park and N. G. Park, *Nanoscale*, 2011, **3**, 4088–4093.
11 H. S. Kim, C. R. Lee, J. H. Im, K. B. Lee, T. Moehl, A. Marchioro, S. J. Moon, R. Humphry-Baker, J. H. Yum, J. E. Moser, M. Grätzel and N. G. Park, *Sci. Rep.*, 2012, **2**, 591.
12 M. M. Lee, J. Teuscher, T. Miyasaka, T. N. Murakami and H. J. Snaith, *Science*, 2012, **338**, 643–647.
13 U. Bach, D. Lupo, P. Comte, J. E. Moser, F. Weissortel, J. Salbeck, H. Spreitzer and M. Grätzel, *Nature*, 1998, **395**, 583–585.
14 J. M. Ball, M. M. Lee, A. Hey and H. J. Snaith, *Energy Environ. Sci.*, 2013, **6**, 1739–1743.
15 M. Liu, M. B. Johnston and H. J. Snaith, *Nature*, 2013, **501**, 395.
16 H. J. Snaith, *J. Phys. Chem. Lett.*, 2013, **4**, 3623–3630.
17 J. Burschka, N. Pellet, S. J. Moon, R. Humphry-Baker, P. Gao, M. K. Nazeeruddin and M. Grätzel, *Nature*, 2013, **499**, 316.
18 Q. Wang, Y. C. Shao, Q. F. Dong, Z. G. Xiao, Y. B. Yuan and J. S. Huang, *Energy Environ. Sci.*, 2014, **7**, 2359–2365.
19 Z. G. Xiao, C. Bi, Y. C. Shao, Q. F. Dong, Q. Wang, Y. B. Yuan, C. G. Wang, Y. L. Gao and J. S. Huang, *Energy Environ. Sci.*, 2014, **7**, 2619–2623.
20 C. Bi, Y. Shao, Y. Yuan, Z. Xiao, C. Wang, Y. Gao and J. Huang, *J. Mater. Chem. A*, 2014, **2**, 18508.
21 A. Dualeh, N. Tétreault, T. Moehl, P. Gao, M. K. Nazeeruddin and M. Grätzel, *Adv. Funct. Mater.*, 2014, **24**, 3250–3258.
22 Q. Chen, H. Zhou, Z. Hong, S. Luo, H. Duan, H. Wang, Y. Liu, G. Li and Y. Yang, *J. Am. Chem. Soc.*, 2014, **136**, 622–625.
23 X. L. Liu, C. G. Wang, I. Irfan, S. J. Yi and Y. Gao, *Org. Electron.*, 2014, **15**, 977.
24 X. Liu, S. Yi, C. Wang, C. Wang and Y. Gao, *J. Appl. Phys.*, 2014, **115**(16), 163708.
25 I. Irfan, A. J. Turinske, Z. N. Bao and Y. Gao, *Appl. Phys. Lett.*, 2012, **101**, 093305.
26 Irfan, H. Ding, Y. Gao, C. Small, D. Y. Kim, J. Subbiah and F. So, *Appl. Phys. Lett.*, 2010, **96**, 243307.
27 Y. Gao, *Mater. Sci. Eng., R*, 2010, **68**(3), 39–87.
28 A. C. Dürr, N. Koch, M. Kelsch, A. Rühm, J. Ghijsen, R. L. Johnson, J.-J. Pireaux, J. Schwartz, F. Schreiber, H. Dosch and A. Kahn, *Phys. Rev. B: Condens. Matter Mater. Phys.*, 2003, **68**, 115428.

29 N. Koch, A. C. Dürr, J. Ghijsen, R. L. Johnson, J.-J. Pireaux, J. Schwartz, F. Schreiber, H. Dosch and A. Kahn, *Thin Solid Films*, 2003, **441**, 145–149.

30 H. Oji, E. Ito, M. Furuta, H. Ishii, Y. Ouchi and K. Seki, *Synth. Met.*, 2001, **121**, 1721–1722.

31 P. Schulz, E. Edri, S. Kirmayer, G. Hodes, D. Cahen and A. Kahn, *Energy Environ. Sci.*, 2014, **7**, 1377.

32 N. Koch, D. Pop, R. L. Weber, N. Böwering, B. Winter, M. Wick, G. Leising, I. V. Hertel and W. Braun, *Thin Solid Films*, 2001, **391**, 81.

33 *Conjugated Polymer and Molecular Interfaces, Science and Technology for Photonic and Optoelectronic Applications*, ed. W. R. Salaneck, K. Seki, A. Kahn and J. J. Pireaux, Marcel Dekker, New York, 2001.